Hindawi
Journal of Nanomaterials
Volume 2017, Article ID 9610419, 11 pages
https://doi.org/10.1155/2017/9610419

Research Article

$H_2Ti_3O_7$ Nanotubes Decorated with Silver Nanoparticles for Photocatalytic Degradation of Atenolol

Mariana Hinojosa-Reyes,[1] Roberto Camposeco-Solís,[2] Facundo Ruiz,[1] Nereyda Niño Martínez,[1] Vicente Rodríguez González,[2] and M. E. Compeán-Jasso[1]

[1]*Facultad de Ciencias, Universidad Autónoma de San Luis Potosí, 78000 San Luis Potosí, SLP, Mexico*
[2]*División de Materiales Avanzados, IPICYT, Instituto Potosino de Investigación Científica y Tecnológica, Camino a la Presa San José 2055, Col. Lomas 4a Sección, 78216 San Luis Potosí, SLP, Mexico*

Correspondence should be addressed to Mariana Hinojosa-Reyes; kittyhinojosa@hotmail.com

Received 7 March 2017; Revised 3 May 2017; Accepted 17 May 2017; Published 27 June 2017

Academic Editor: Nageh K. Allam

The photocatalytic degradation/adsorption process of the β-blocker atenolol (ATL) under UV irradiation is described using two types of silver decorated catalysts: silver/titania and silver/titanates. The silver ions were reduced on the surface of TiO_2-P25-*Degussa* using gallic acid. Silver/titanates were prepared by a microwave-assisted hydrothermal method using the silver/titania as the starting material to obtain the hydrogen titanate ($H_2Ti_3O_7$) structure with tubular morphology. These materials were characterized by X-ray diffraction, UV-Vis spectroscopy, N_2 physisorption, temperature programmed reduction, TEM, and FTIR spectroscopy. During the photocatalytic process, the ATL molecules were completely converted to amino-diol byproducts. It is the first time that these materials have been applied during the photocatalytic process in the degradation of pharmaceuticals products. The success of the silver nanoparticles (2 nm) consists of the homogeneous distribution over the surface of titanate nanotubes inhibiting the hole/electron recombination promoting the oxidation process. The $Ag@H_2Ti_3O_7$ with a concentration of silver as 1.0% shows the highest adsorption/degradation of ATL than the $Ag@TiO_2$ and the P25-*Degussa*. The great performance in the reuse test consists in the strong attachment of the silver nanoparticles on the titanium surface that inhibits the silver lixiviation during the photocatalytic tests.

1. Introduction

Titanium dioxide is a material widely used due to the stability of its chemical structure, low toxicity, low cost, and physicochemical properties [1]. Due to these properties, it has been applied in anticorrosion problems, self-cleaning coatings, paints for solar cells, and catalysis applications [2]. Tubular structures have received particular interest since the carbon nanotubes were discovered; they are very interesting structures because of their high surface/volume ratios and they are size-dependent; these properties are enhanced when TiO_2 nanotubes are doped with other elements or functionalizing their surface with metallic nanoparticles.

The TiO_2 nanotubes are a semiconductor with a large surface area with respect to TiO_2 crystals, which have been applied in dye-sensitized solar cells, water photoelectrolysis, photo-degradation of hazardous materials, and catalysis, among other applications [3]. Powdered titanium dioxide has been efficiently used to eliminate a large variety of organic pollutants present in water; among the catalysis applications it has been applied during the photocatalytic degradation of organic compounds; recent studies have reported the removal of dyes by combining adsorption and photocatalysis processes [4]. Emerging Contaminants (EC) are present in a wide range of pharmaceuticals and personal care products (PPCPs) among which are cosmetics, antimicrobials, antibiotics, analgesics, antidepressants, hypertensives (β-blockers), and many other chemicals that are widely used on a daily basis for various purposes [5]. Within the hypertensives β-blockers we select the β_1 receptor antagonist, atenolol (ATL), due to it having been used primarily for the treatment of cardiovascular diseases for more than thirty years. Due to its extensive usage and limited human metabolism, ATL was widely detected in sewage effluents and surface

waters, usually with a concentration ranging from ngL^{-1} to μgL^{-1}. Previous researchers have demonstrated that ordinary wastewater treatments cannot remove ATL effectively. Furthermore, many studies have provided evidence that ATL could inhibit the growth of human embryonic cells and was ecotoxic to freshwater species. Therefore, it is essential to develop advanced treatment technologies for ensuring effective elimination of ATL in wastewaters before releasing into natural waters [6]. Treatment plants are not able to degrade residues of this nature, and, as a result, they are introduced into the aquatic environment [7]; over time these chemical residues cause many affectations on aquatic organisms and generate human diseases.

An alternative technology and cost-effective solution to deal with this kind of contaminants is the use of the advanced oxidation processes (AOPs) that are based in the hydroxyl radicals able to oxidize pollutants into harmless end-products, which could result in a full mineralization (CO_2, H_2O, and inorganic ions) [8].

In this work, we report for the first time the photocatalytic degradation/adsorption of atenolol in aqueous phase using TiO_2 nanotubes ($H_2Ti_3O_7$) modified with silver nanoparticles. Ag/titanium materials have particular attention for their low cost and the superior properties of silver [9]. On the other hand, the main advantage of TiO_2 nanotubes is their high surface area that enhances the photocatalytic/adsorption processes; at the same time, the silver presence inhibits the hole/electron recombination that enhances the photoactivity regarding the well-known P25-*Degussa*.

2. Experimental Section

2.1. Catalysts Preparation. The Ag@TiO_2 catalysts were prepared by dissolving 2.5 g of TiO_2-P25-*Degussa* in 250 mL of deionized water and sonicated for 15 min; then $AgNO_3$ (99.3%, Fermont) 1×10^{-3} M was added to reach three different concentrations: 0.5, 1.0, and 2.5% wt; then gallic acid (97.5–102.5%, Sigma-Aldrich) 6×10^{-4} M was added. The pH of the reaction media was adjusted to 9 by adding NH_4OH, and the obtained sludge was kept under magnetic stirring for 1 hour. HNO_3 was incorporated to neutralize the solution; four hours later, two phases were formed (liquid-solid); the solid phase was removed and dried for four hours at 80°C.

The synthesis of Ag@TiO_2 nanotubes was carried out by a microwave-assisted method (Eyela MWO-1000 Wave Magic). 1.5 g of the previously obtained samples (Ag@TiO_2) was placed into a 150 mL Teflon vessel with 60 mL of NaOH 10 N. The reaction mixture was placed in a microwave tube and microwaved for 4 hours at a power output of 195 W and a continuous stirring of 600 rpm. The temperature reached was 140°C. The solid was washed with distilled water until the pH was neutralized and finally the solid was dried at 100°C for 2 hours.

Samples were identified as Ag@TiO_2-*X* for the case of silver/titania and Ag@$H_2Ti_3O_7$-*X* for the case silver/titanates; *X* indicates the silver concentration in % wt.

2.2. Characterization Techniques. The Ag@TiO_2 and Ag@$H_2Ti_3O_7$ catalysts were characterized by X-ray diffraction in order to identify the crystalline phases using an X-ray diffractometer SmartLab RIGAKU with CuKα radiation (1.5404 Å). Diffuse reflectance UV-Vis spectra of the photocatalysts were obtained using a Cary 5000 (UV-Vis-NIR) spectrophotometer; spectralon Teflon (from Agilent) was used as a reference blank and the band gap energy was determined by using the Kubelka-Munk method. The physical adsorption of N_2 at −196°C was carried out using a NOVA 3200e, Surface Area & Pore Size Analyzer by Quantachrome Instruments. Samples were previously outgassed at 200°C during 14 hours. The Brunauer-Emmett-Teller method (BET method) was used to calculate the specific surface area. Temperature Programmed Reduction (TPR) was performed in a ChemBET TPR/TPD chemisorption analyzer by Quantachrome Instruments using an interval of temperature ranging from Room Temperature (RT) to 600°C with a rate of $10^{\circ}C\,min^{-1}$ and flow of 30 mL min^{-1} of H_2 (10%)/Ar gas. Morphology of the Ag catalysts was obtained by Scanning Electronic Microcopy using a JEOL JSM-6510 microscope at an accelerating voltage of 30 kV.

Infrared (IR) spectra were obtained using a Shimadzu IRTracer-100 spectrophotometer equipped with a Praying Mantis for DRIFT spectroscopy and a low/high-temperature reaction chamber by Harrick. In each experiment, approximately 25 mg of dried sample was packed in the sample holder. IR measurements were carried out, under a constant flow of N_2 (30 mL/min), from RT to 600°C in steps of 100°C.

Diffuse reflectance UV-Vis spectra of the catalysts were obtained using a CARY 5000 (UV-VIS-NIR) spectrophotometer equipped with a Praying Mantis and a high-temperature reaction chamber (Harrick) and it was recorded during the activation thermal treatment, from 25°C and every 50°C until reaching 600°C; in each experiment, approximately 25 mg of the dried sample was packed in the sample holder under constant N_2 flow (30 mL min^{-1}).

The samples were examined by Transmission Electron Microscopy (TEM) in a Tecnai FEI 300 operated at 300 kV. The samples were suspended in isopropanol and then sonicated for 5 min. Finally, the samples were mounted in a Cu TEM grid. The particle size distribution histograms for the catalysts were obtained from the measurements of about 200 particles. The average particle diameter (d_s) was calculated using the following formula: $d_s = \sum n_i d_i / \sum n_i$, where n_i is the number of particles of diameter d_i.

2.3. Photocatalytic Evaluation. A standard solution of atenolol (>98%, Sigma) with 10 ppm was used to evaluate the photocatalytic activity of the Ag photocatalysts. Photocatalytic experiments were carried out in triplicate in a reactor with 200 mL of ATL at 10 ppm in vigorous stirring under 90 minutes of dark adsorption; after that, the $UV_{365\,nm}$ irradiation was turned on. The full time of reaction with irradiation was 210 minutes. Aliquots were taken since the start of the reaction and subsequently every 30 minutes; then they were filtered with a Nylon membrane of 0.45 μm by Pall.

Firstly, the catalyst concentration was optimized using the following: 175, 250, and 375 mg L^{-1}, corresponding to 35, 50, and 75 mg of catalyst into 200 mL of contaminant solution.

Table 1: Physicochemical properties of Ag materials.

Sample	Surface area ($m^2\ g^{-1}$)	E_g (eV)	Crystalline phases
Ag@TiO_2 0.5	52.1	2.48	Anatase, rutile
Ag@TiO_2 1.0	51.4	2.41	Anatase, rutile
Ag@TiO_2 2.5	52.9	2.25	Anatase, rutile
Ag@$H_2Ti_3O_7$ 0.5	287.1	2.76	$H_2Ti_3O_7$
Ag@ $H_2Ti_3O_7$ 1.0	297.1	2.87	$H_2Ti_3O_7$
Ag@ $H_2Ti_3O_7$ 2.5	188.2	2.73	$H_2Ti_3O_7$

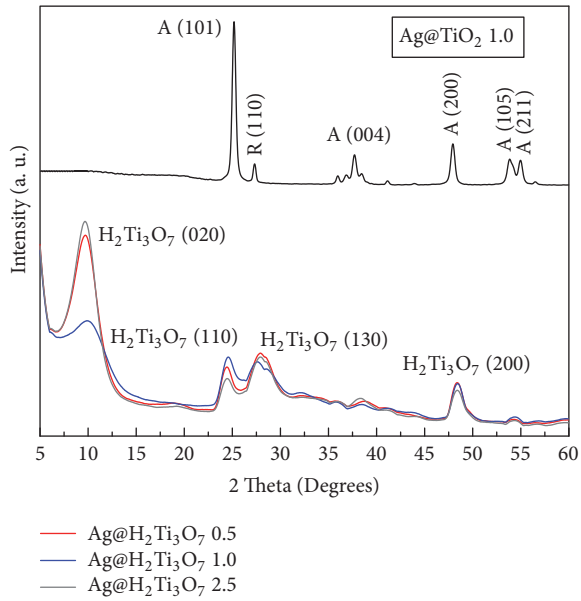

Figure 1: X-ray diffractograms of the silver catalysts. At the top is of the P25-Degussa and at the bottom is of the Ag@$H_2Ti_3O_7$.

The monitoring of the reaction consists in the measurement of the intensity band at 223 nm characteristic of the ATL molecule using an UV-Vis Ocean Optics USB4000 spectrophotometer. To monitor the Total Organic Carbon (TOC), samples were taken from the reaction at beginning, after adsorption and the end of the photocatalytic reaction, using a TOC-V_{CPN} Total Organic Carbon Analyzer by Shimadzu. The Ag lixiviation during the photocatalytic reactions was measured by using an atomic absorption spectrophotometer AA 7000 by Shimadzu. A cyclic test was carried out with the Ag@$H_2Ti_3O_7$ 1.0 catalyst to evaluate the reusability and stability of the material.

3. Results and Discussion

3.1. Physicochemical Properties

3.1.1. X-Ray Diffraction. The X-ray diffractograms are shown in Figure 1. At the top the Ag@TiO_2 1.0 is presented; it is possible to see only the pattern corresponding to P25-*Degussa* with the presence of anatase (JCPDS 04-002-2678) and rutile (JCPDS 70-7347) crystalline phases. At the bottom, the Ag@$H_2Ti_3O_7$ diffractograms are presented. We can observe the total conversion from anatase/rutile to $H_2Ti_3O_7$ (JCPDS 47-0651) titanate nanotubes [10] after microwave-assisted method was used [11]. In the same way, the presence of peaks related to metallic silver or silver oxides is not present; this could be due to a low silver concentration or the homogeneous silver nanoparticles dispersion. From Figure 1 at the bottom, in the case of Ag@$H_2Ti_3O_7$ 1.0 sample, it is evident that the peak corresponding to the (020) planes is less intense than the other samples; it is due to a less concentration of sodium ions. These sodium ions come from the basic conditions (NaOH). This change may arise due to the complete exchange of sodium ions by protons after extensive washing with acid [12].

3.1.2. UV-Vis Spectroscopy. The UV-Vis spectra of the Ag catalysts are shown in Figure 2. Figure 2(a) corresponds to materials synthesized by reduction method. In the first instance, it is observed the silver surface plasmon resonance (SPR) which is shifted to higher wavelength according to the silver concentration from 0.5, 1.0 and 2.5% wt. corresponding to 500, 480, and 459 nm, respectively; also, a higher intensity of the SPR band was detected in the sample with higher silver content. It has been reported a value of 480 nm for Ag nanoparticles and its value decreases for small nanoparticles [13, 14]. Figure 2(b) corresponds to titanate nanotubes; in this case, the SPR is less evident. This situation could be attributed to silver nanoparticles that are found into nanotube and a lower concentration is on the surface of its structure.

Band gap values of the catalysts were determined by using the Kubelka-Munk method; these values are reported in Table 1. For the case of Ag@TiO_2 materials, the band gap energy (E_g) has values of 2.48, 2.41, and 2.25 eV; it is possible to observe that E_g is inversely proportional to silver concentration. For the case of samples prepared by reduction followed by hydrothermal method, the band E_g shows values in the range of 2.7 to 2.8 eV. It is important to mention that E_g of the P25 is notably affected by the silver concentration since P25-*Degussa* has a well-known value of 3.2 eV [15].

An additional UV-Vis-NIR DRS with temperature increasing experiment was carried out to elucidate the behavior of the Ag@$H_2Ti_3O_7$ sample at different temperatures in the range of 25 to 400°C; see Figure 3. In this context, a dramatic change in the behavior in the range of temperatures 200 to 300°C is appreciated; around these temperatures, collapsing of the nanotube structure happens [16]. In addition, from a temperature of 25°C, a surface resonance plasmon at 450 nm corresponding

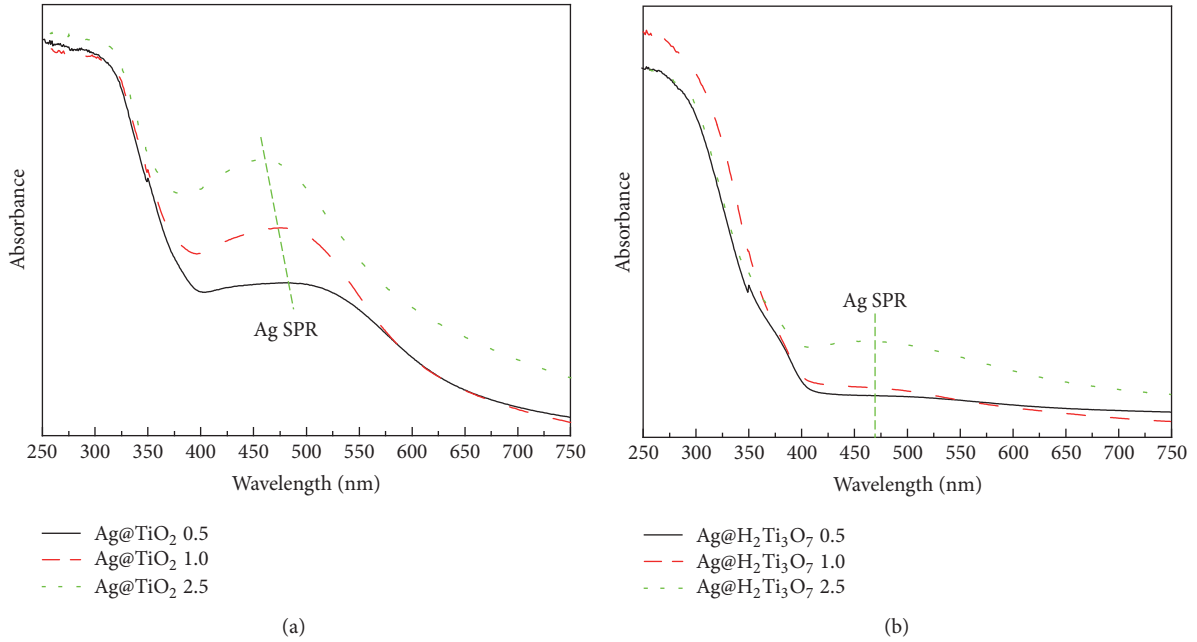

Figure 2: UV-Vis spectra of the silver catalysts of (a) $Ag@TiO_2$ and (b) $Ag@H_2Ti_3O_7$.

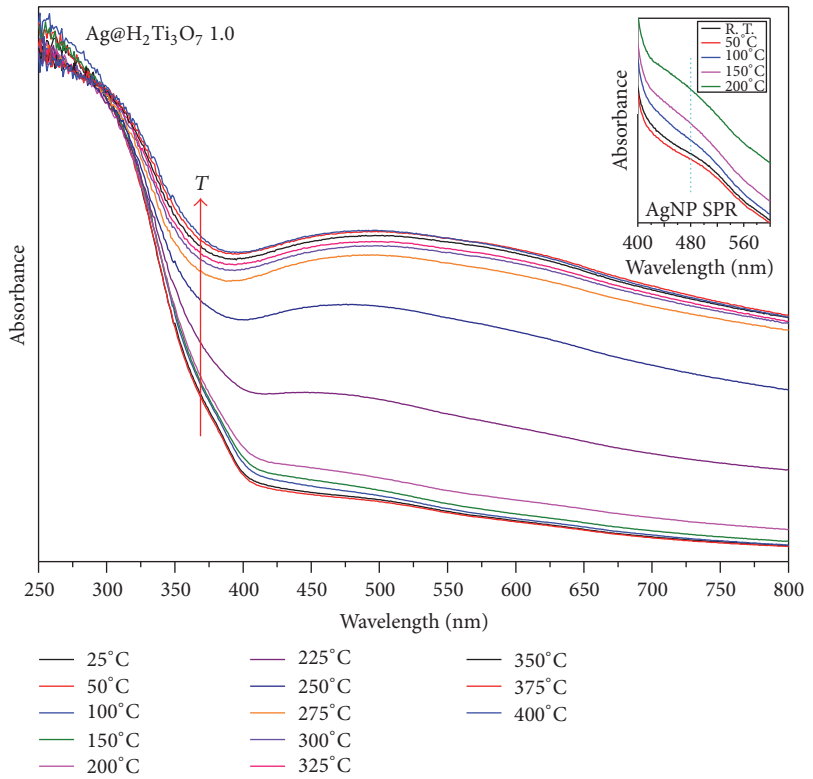

Figure 3: UV-Vis-NIR DRS collected spectra for the $Ag@H_2Ti_3O_7$ 1.0 sample with temperature increasing from 25 to 400°C. Inset corresponding to the SPR of the AgNPs from RT to 200°C.

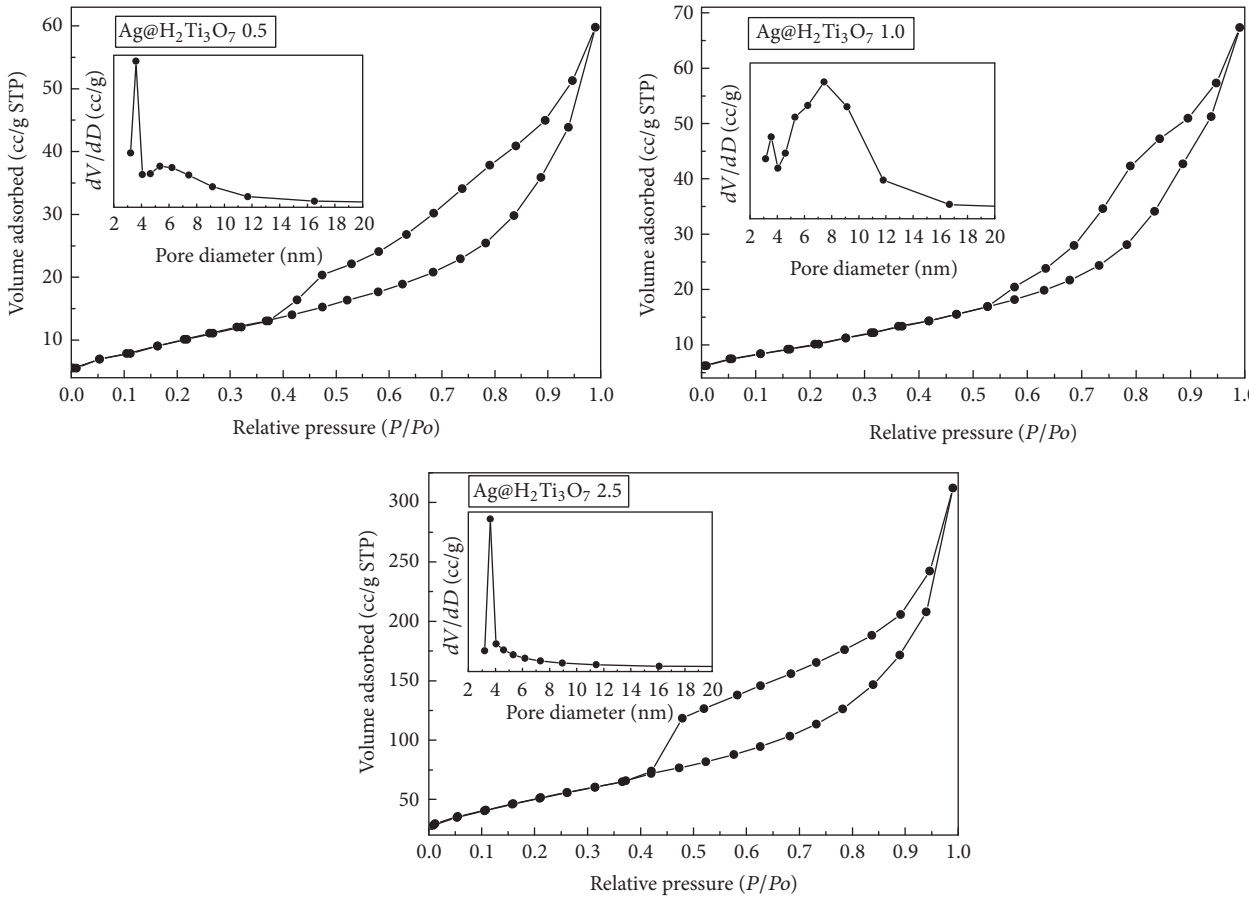

Figure 4: Adsorption-desorption nitrogen isotherms of the $Ag@H_2Ti_3O_7$ catalysts. Insets show the size pore distribution.

to silver nanoparticles is observed; as the temperature increases, this band increases its intensity and moves to higher wavelengths. According to the inset of Figure 3 is corroborated the presence of the Ag nanoparticles inside the nanotube structure, and according to temperature increases, these Ag nanoparticles get out to the surface. Therefore always the SPR is present in all the temperatures range; see inset of Figure 3.

3.1.3. Nitrogen Physisorption. The nitrogen physisorption isotherms are shown in Figure 4. The $Ag@H_2Ti_3O_7$ samples present high surface area values: 287, 297, and 188 $m^2\,g^{-1}$ for Ag concentrations of 0.5, 1.0, and 2.5% wt, respectively (see Table 1). The $Ag@TiO_2$ 1.0 presents the highest surface area. According to IUPAC classification, nanotubes have type IV isotherms and H3 hysteresis loop [17]. This kind of hysteresis is associated with aggregates of plate-like particles giving rise to slit-shaped pores [17]. Pore size distribution, of the three samples, was analyzed using the Barrett–Joyner–Halenda (BJH) method; see insets of Figure 4. It is important to notice that the $Ag@H_2Ti_3O_7$ 1.0 sample presents two pore size distributions, one centered at around 4 nm and another one at around 4 nm. The other samples, with a silver concentration of 0.5 and 2.5, have the pore size distribution centered at approximately 4 nm. For the $Ag@H_2Ti_3O_7$ 1.0 sample, we found it has the less concentration of sodium ions (after washing); this fact could explain why this sample has a bimodal pore size distribution. We think that the 4 nm pores correspond to the inside diameters of titanate nanotubes and the other larger pores (8 nm) are the space between the nanotubes in the nanotubes-bundles [18].

For comparison the $Ag@TiO_2$ materials also were measured and have values in order of 52 $m^2\,g^{-1}$ (see Table 1), almost the same value corresponding to well-known bare TiO_2-P25-*Degussa* [18].

3.1.4. Temperature Programmed Reduction. The thermograms corresponding to the temperature reduction of the silver photocatalysts prepared by hydrothermal assisted method are shown in Figure 5. Specifically for the high silver concentration sample ($Ag@H_2Ti_3O_7$ 2.5), the thermograms have a well-defined peak that begins at 149° and finishes at 190°C with a maximum at 170°C; this peak corresponds to the reduction of Ag^{1+} to Ag^0. For the sample $Ag@H_2Ti_3O_7$ 0.5, this peak is not so evident, but it still presents a band between 150° and 350°C, which also corresponds to the reduction of silver, but due to the low silver concentration and its interaction with titanium support, it is shifted to higher temperatures.

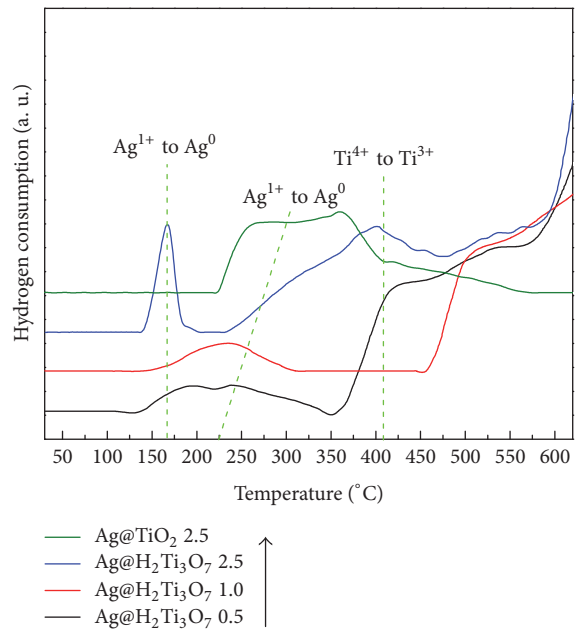

FIGURE 5: Temperature programmed reduction graph of the silver-titanium catalysts.

The $Ag@TiO_2$ 2.5 result is presented as a reference and it shows a peak around 225 and 400°C that also corresponds to the reduction of Ag^{1+} to Ag^0. At temperatures above of 400°C, it is possible to observe how the reduction of the support starts (Ti^{4+} to Ti^{3+}) [19]. It is important to mention that the titanium reduction temperature varies according to the nanoparticles concentration [20]; at the higher temperature, it is possible to observe a lower interaction with silver nanoparticles.

In Figure 6(a) is shown an STEM-HAADF image of the $Ag@H_2Ti_3O_7$ 1.0 sample. In this image, we could observe a well-defined morphology of the nanotubes-$H_2Ti_3O_7$ structure. This image corroborates the homogeneous silver deposition on the nanotube structure. Silver is found forming spherical nanoparticles (white dots), homogeneously distributed in space and size. The $Ag@TiO_2$ material consists in agglomerates of spherical nanometric particles of TiO_2 (P25-*Degussa*). Once the $Ag@TiO_2$ samples were treated by the hydrothermal method, there is a complete conversion from spherical nanoparticles to large nanotubes corresponding to $H_2Ti_3O_7$ stoichiometry according to XRD information.

Frequency histograms of size and diameter are reported for Ag nanoparticles and nanotubes; see Figures 6(b) and 6(c); where the Ag nanoparticles average size is 2.23 nm; therefore, the reduction method guarantees homogeneous silver size dispersion. According to the frequency histogram for diameter nanotubes, the average diameter is 6.6 nm.

According to literature, for a first time is reported the least size of Ag nanoparticles supported on TiO_2 nanotubes, since the nanoparticles size reported is on the order of 5 or higher than 10 nm [21–23]. With respect to the measurements of nanotubes, we obtained a lesser diameter size than what was reported in the literature, which is an average of 8–10 [21], 10–20 [22], and 60–70 nm [23]. These nanotubes applied firstly in the photocatalytic degradation of dye or model molecules in this research are successfully used during the photocatalytic adsorption/degradation of the pharmaceutical atenolol.

The hydroxyl groups present in the $H_2Ti_3O_7$ surface are shown in Figure 7. The part (a) corresponds to nanotube decorated with silver and shows two bands located at 3653 and 3715 cm^{-1}, while for the bare $H_2Ti_3O_7$ nanotube two bands are shown located at 3658 and 3717 cm^{-1}; see Figure 7 part (b). These bands are assigned to hydrogen bonded to adjacent OH groups in terminal positions due to the stretching modes of Ti-OH [24, 25]. By comparison, the $H_2Ti_3O_7$ bands have a major intensity regarding the $Ag@H_2Ti_3O_7$ material; this is directly associated with Ag nanoparticles that are anchored over these OH groups.

According to structural and surface properties of Ag-nanotubes, these have been applied successfully during the photocatalytic degradation/adsorption of atenolol.

3.2. Photocatalytic Results. The previously synthesized $Ag@H_2Ti_3O_7$ nanotubes were tested during the photocatalytic degradation of ATL. First, an optimization of the catalyst was made using the concentrations of 175, 250, and 375 mg L^{-1}. Results indicate that optimal load is 250 or 375 mg L^{-1}, but for practical purposes, it was chosen a concentration of 250 mg L^{-1}. With this load is reached a final degradation of 80%, which corresponds to the same adsorbed quantity during the dark conditions; see Figure 8(a). The evaluation of the rest of materials with this load indicates a low degradation/adsorption of 50% for $Ag@H_2Ti_3O_7$ 0.5 and 10% for $Ag@H_2Ti_3O_7$ 2.5; see Figure 8(b). The best photocatalytic degradation is due to the $Ag@H_2Ti_3O_7$ 1.0 sample and the catalyst with bigger pore diameter

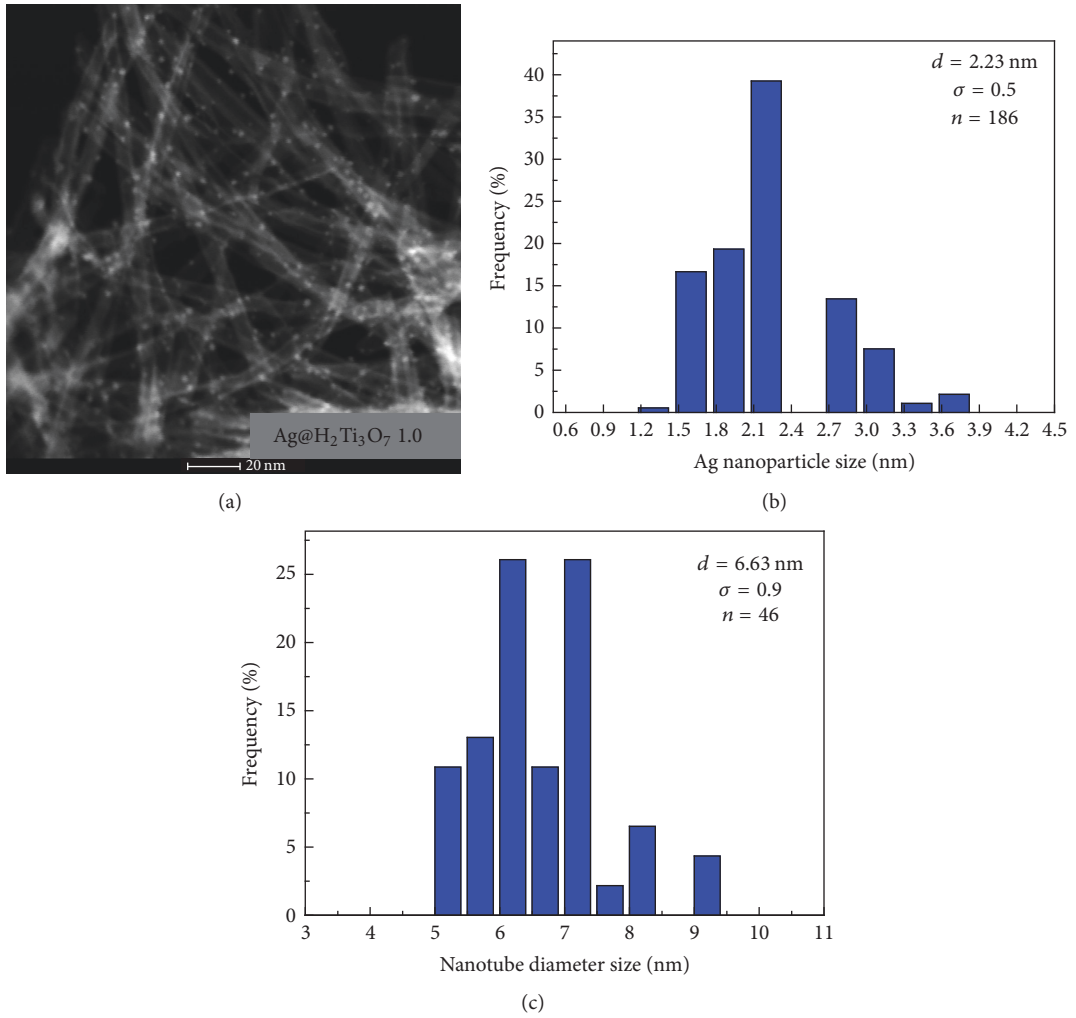

FIGURE 6: (a) STEM-HAADF image for $Ag@H_2Ti_3O_7$ 1.0 sample. Frequency histograms for (b) Ag nanoparticles size and (c) nanotube diameter size.

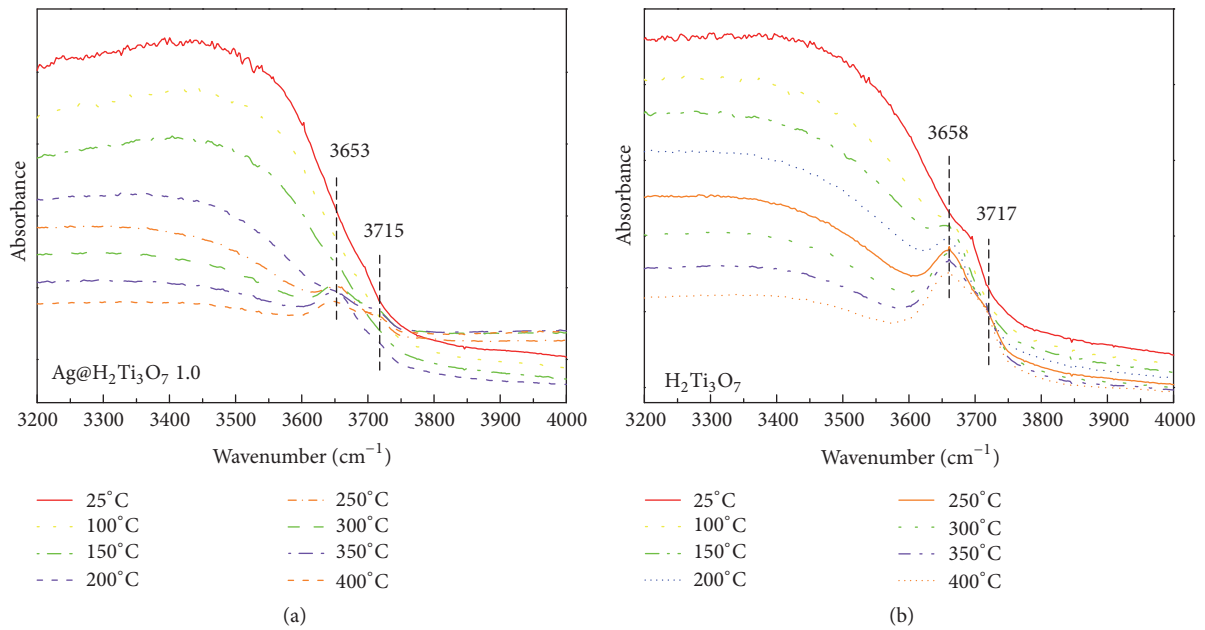

FIGURE 7: FTIR spectra of (a) $Ag@H_2Ti_3O_7$ 1.0 and (b) $H_2Ti_3O_7$.

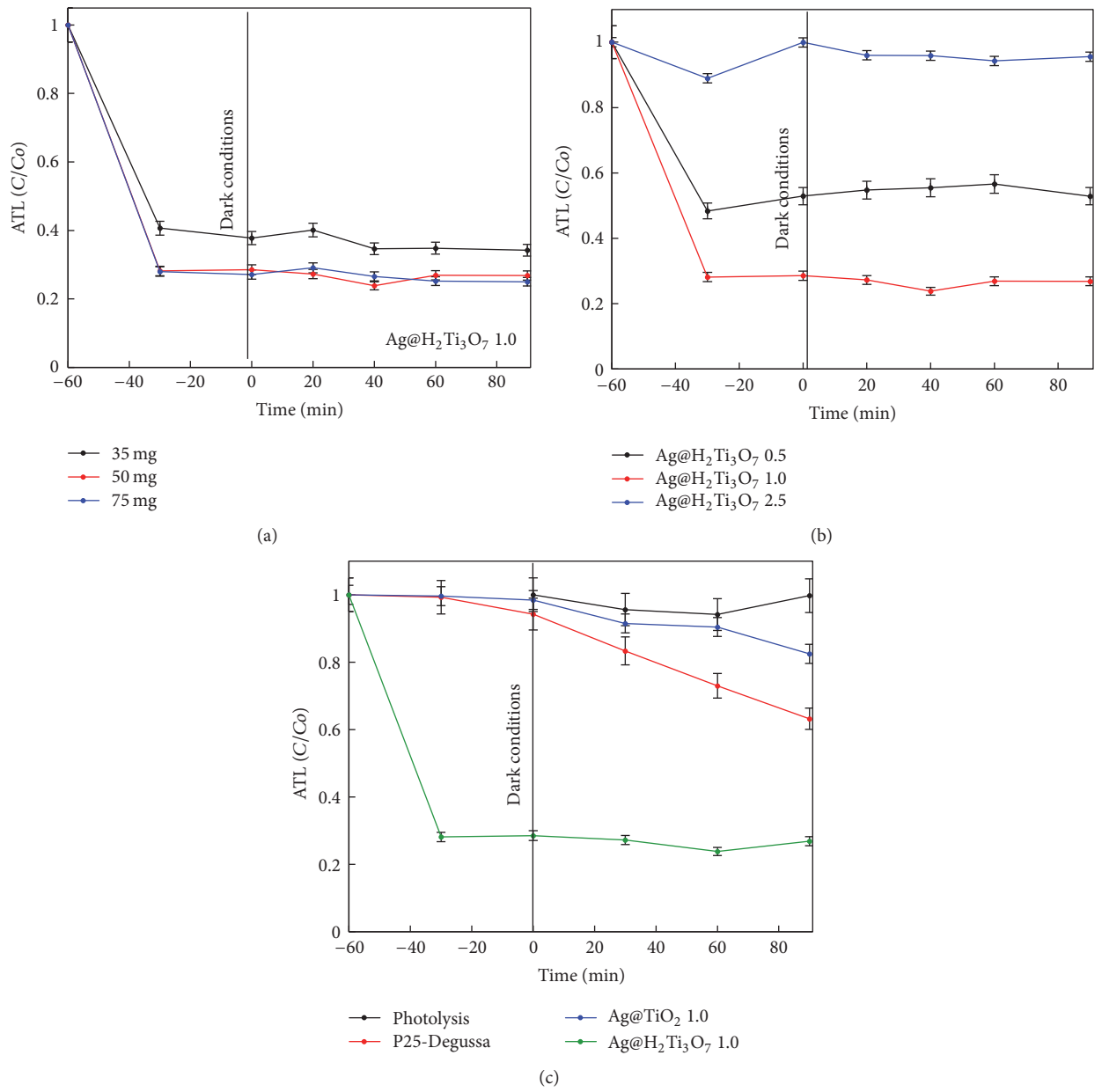

FIGURE 8: (a) Optimization of the silver load of photocatalyst using $Ag@H_2Ti_3O_7$ 1.0., (b) 50 mg of the photocatalyst, and (c) comparative behavior regarding TiO_2 references and photolysis for the 200 mL of ATL degradation at 10 ppm and pH normal.

and with the highest surface area. As already mentioned, the highest surface area is correlated with minor sodium ions concentration presents in the $H_2Ti_3O_7$ structure. Therefore, a minor sodium ions concentration represents an enhancement during the adsorption/degradation of the ATL molecule.

For comparative purposes, Figure 8(c) shows the behavior of the P25-*Degussa* to compare with the $Ag@TiO_2$ 1.0, $Ag@H_2Ti_3O_7$ 1.0, and it respective photolysis. Photolysis shows a negligible degradation. The P25-*Degussa* and $Ag@TiO_2$ 1.0 show a minimal adsorption under dark conditions of around 3%. Once the UV light is turned on, the $Ag@TiO_2$ 1.0 shows a final degradation of 20%, while P25-*Degussa* is around 30% of the ATL molecule. Although it is well known that silver nanoparticles avoid the hole-electron recombination, in this case, the commercial TiO_2 shows a greater behavior than the silver modified catalyst; this is due to gallic acid precedent from the synthesis that was not removed and could cover the active sites of the TiO_2. At the same time the $Ag@H_2Ti_3O_7$ 1.0 shows 80% of adsorption and once the ATL is adsorbed onto the nanotube surface is followed the formation of the respective byproducts.

3.2.1. TOC Analysis. The TOC analysis for the degradation of ATL molecule using the nanotubes decorated with silver reveals a maximum mineralization of 50% for the

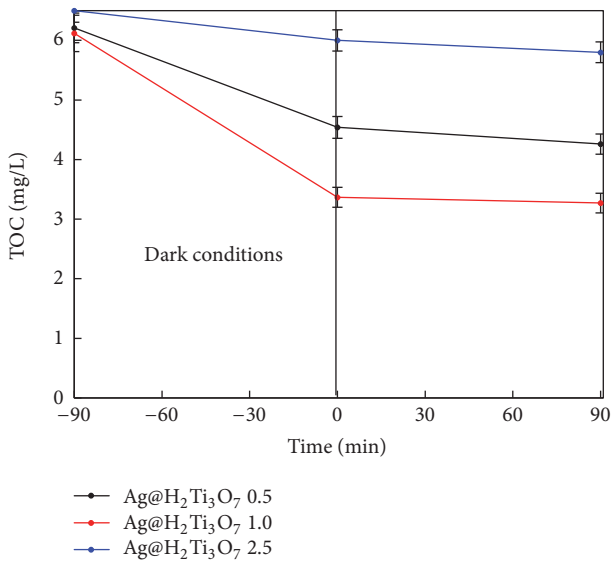

Figure 9: TOC (mg/L) measurements during the photocatalytic degradation of ATL using the $Ag@H_2Ti_3O_7$ catalysts at pH 7.

$Ag@H_2Ti_3O_7$ 1.0 catalyst, 25% for the $Ag@H_2Ti_3O_7$ 0.5, and less than 5% for the $Ag@H_2Ti_3O_7$ 2.5 material (Figure 9). According to UV-Vis spectroscopy measurements that indicate a maximum degradation of 80%, for the $Ag@H_2Ti_3O_7$ 1.0 catalyst, only a 50% of the ATL is mineralized into CO_2 and water; the remaining 30% is converted into a simple molecule, the byproduct amino-diol [26, 27]. The photocatalytic process has a high efficiency when there is a higher percentage of adsorption. Thus, the novelty of the silver decorated nanotubes synthesized in this research has a good performance during the degradation of atenolol molecule.

3.2.2. Silver Lixiviation Test. The stability of the $Ag@H_2Ti_3O_7$ catalysts was evaluated through its lixiviation by atomic absorption; aliquots were taken at the end of the photocatalytic reaction (4 hours). Table 2 reveals the concentration of Ag (ppm) and the corresponding percentage. The aliquot taken for the $Ag@H_2Ti_3O_7$ 0.5 sample shows a final Ag concentration of 0.0053 ppm equivalent to 0.4% of full lixiviation. The $Ag@H_2Ti_3O_7$ 1.0 sample shows a full lixiviation of 1.2% and the $Ag@H_2Ti_3O_7$ 2.5 shows a full lixiviation of 6.4%. The obtained percentages are negligible and, with this result, we can affirm that hydrothermal assisted method guarantees catalysts with silver nanoparticles strongly attached to the TiO_2 nanotubes.

3.2.3. Reusability Test. The behavior of the ATL degradation using the $Ag@H_2Ti_3O_7$ 1.0 can be seen in Figure 10. After 30 min of adsorption during dark conditions, a decrease of the UV band is observed occurring at 225 nm and 276 nm. After that, a minimal degradation is observed at the end of adsorption process; during the 60 and 90 minutes of photocatalytic degradation an additional band at 248 nm is observed; this band is assigned to the byproducts formed during the photocatalytic process and according to literature corresponds to the formation of an amino-diol [26, 27]. Amino-diol is a byproduct of ATL fragmentation due to the participation of hydroxyl radicals ($OH^{\bullet}$) and irradiation UV effect during the photocatalytic degradation reaction. It is important to mention that an amino-diol is the simplest and less contaminant molecule compared to initial ATL.

Table 2: Silver lixiviation test during the photocatalytic degradation of ATL at 10 ppm and pH normal.

Sample	Ag concentration (ppm)	Lixiviation (%)
$Ag@H_2Ti_3O_7$ 0.5	0.0053	0.4
$Ag@H_2Ti_3O_7$ 1.0	0.0282	1.2
$Ag@H_2Ti_3O_7$ 2.5	0.0805	6.4

To corroborate the stability of the most active $Ag@H_2Ti_3O_7$ titanate, a reusability test of three cycles was made (see Figure 10). In the first cycle is observed an immediate adsorption around 50% and we can see the characteristic ATL band at 225 nm. After the dark absorption process and when the UV lamp is turned on, the 225 nm remains almost constant until the first 90 min of photocatalytic reaction and it starts to appear a shoulder at 248 nm corresponding to amino-diol byproduct.

Once the first cycle was completed, the catalyst was recovered, dried, and used again in a second cycle (Figure 10). In this graph, a lower adsorption is observed around 20%, and immediately after that the lamp turns on; it starts the appearance of shoulder corresponding to the byproducts. In the third cycle, the initial dark adsorption is negligible.

Therefore, with this experiment could be verified the stability and reusability of the $Ag@H_2Ti_3O_7$ 1.0 catalyst. According to that when the catalyst is reused, the ATL conversion to amino-diol is accelerated. This is a good result due to amino-diol being simpler and less contaminant than ATL initial molecule.

4. Conclusions

The silver/titanates nanotubes ($Ag@H_2Ti_3O_7$) show a high efficiency of adsorption at around 80% for β-blocker ATL, part of the ATL molecules adsorbed onto the silver/titanates surface area transformed to amino-diol and 50% of the ATL is mineralized into CO_2 and water. The photocatalytic behavior of this kind of material could be due to the high increase of its surface area; in this case, it is almost 300 $m^2\,g^{-1}$; this increase in the surface area is induced for the hydrothermal assisted microwave method and also due to the fewer sodium ions concentration. Also, this behavior could be attributed to the presence of silver nanoparticles and they are responsible for avoiding the recombination of the electron/hole pair. The silver/titanates results reported in this work indicate that they are good candidates for use in wastewater treatment plants to eliminate PPCPs and they could avoid human and marine species diseases.

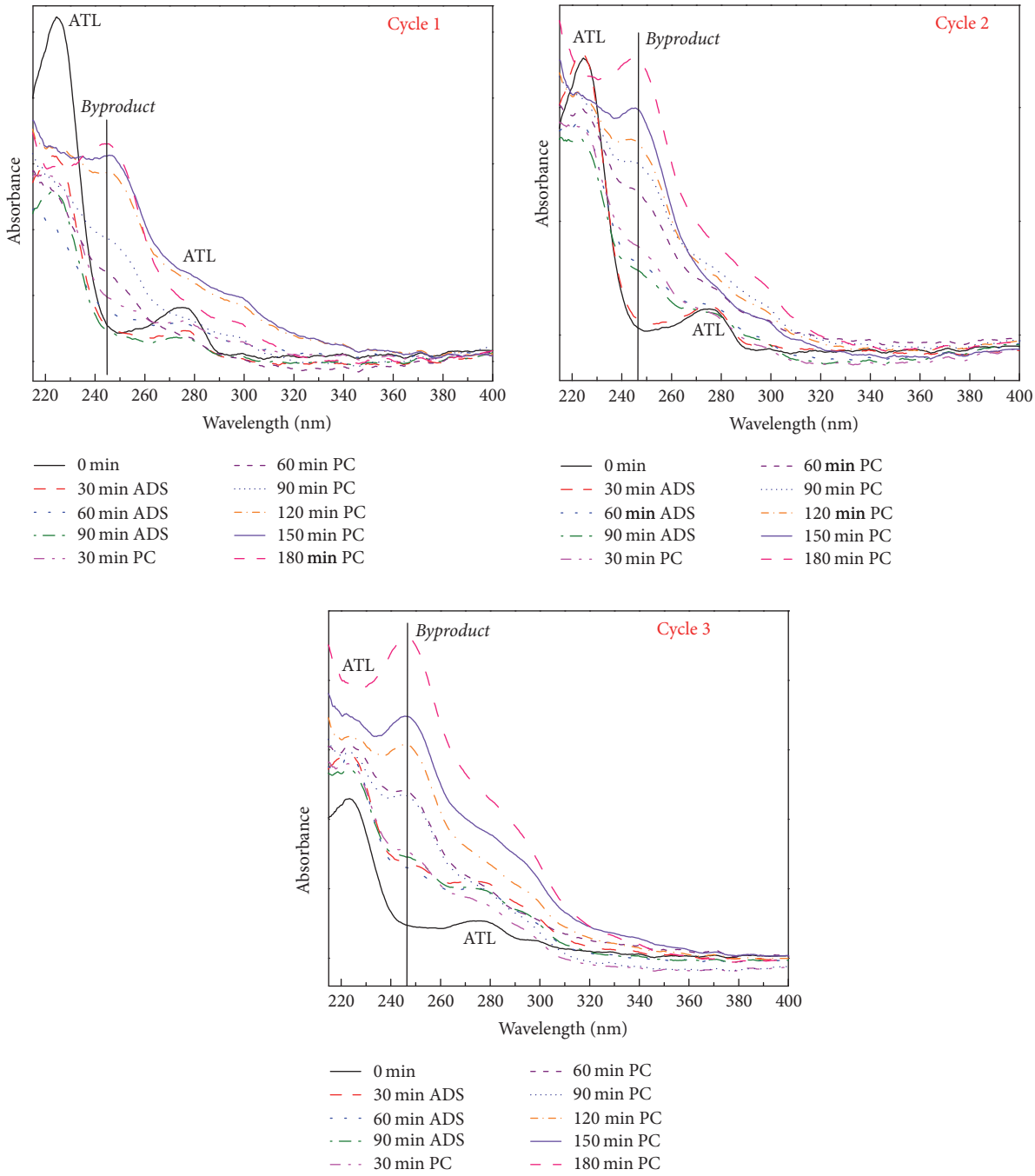

FIGURE 10: Reusability test (three cycles) during the photocatalytic degradation of ATL using the $Ag@H_2Ti_3O_7$ 1.0 catalyst.

Conflicts of Interest

The authors declare that there are no conflicts of interest regarding the publication of this paper.

Acknowledgments

This work is supported by the SEP CONACYT-2014 S-2780, CB-2011/169597, and CB-2010-01-153675 projects. M. Hinojosa-Reyes is thankful for postdoctoral fellowship DSA/103.5/15/12695 funding by PRODEP. The authors also thank the LINAN-IPICYT for the equipment and infrastructure provided. The authors wish to thank B. A. Rivera Escoto, R. F. Araujo Martínez, and G. M. Loredo Becerra for their valuable support. Financial support for the payment of the processing charges was made by "Programa para el Desarrollo Profesional Docente para el Tipo Superior" (PRODEP).

References

[1] S. M. Gupta and M. Tripathi, "A review of TiO_2 nanoparticles," *Chinese Science Bulletin*, vol. 56, no. 16, pp. 1639–1657, 2011.

[2] D. V. Bavykin, J. M. Friedrich, and F. C. Walsh, "Protonated titanates and TiO_2 nanostructured materials: synthesis, properties, and applications," *Advanced Materials*, vol. 18, no. 21, pp. 2807–2824, 2006.

[3] G. K. Mor, K. Shankar, M. Paulose, O. K. Varghese, and C. A. Grimes, "Use of highly-ordered TiO_2 nanotube arrays in dye-sensitized solar cells," *Nano Letters*, vol. 6, no. 2, pp. 215–218, 2006.

[4] A. Sandoval, C. Hernández-Ventura, and T. E. Klimova, "Titanate nanotubes for removal of methylene blue dye by combined adsorption and photocatalysis," *Fuel*, vol. 198, pp. 22–30, 2016.

[5] Q. Sui, X. Cao, S. Lu, W. Zhao, Z. Qiu, and G. Yu, "Occurrence, sources and fate of pharmaceuticals and personal care products in the groundwater: a review," *Emerging Contaminants*, vol. 1, no. 1, pp. 14–24, 2015.

[6] Y. Ji, L. Zhou, C. Ferronato et al., "Photocatalytic degradation of atenolol in aqueous titanium dioxide suspensions: kinetics, intermediates and degradation pathways," *Journal of Photochemistry and Photobiology A: Chemistry*, vol. 254, pp. 35–44, 2013.

[7] A. Nikolaou, S. Meric, and D. Fatta, "Occurrence patterns of pharmaceuticals in water and wastewater environments," *Analytical and Bioanalytical Chemistry*, vol. 387, no. 4, pp. 1225–1234, 2007.

[8] R. Thiruvenkatachari, S. Vigneswaran, and I. S. Moon, "A review on UV/TiO_2 photocatalytic oxidation process," *Korean Journal of Chemical Engineering*, vol. 25, no. 1, pp. 64–72, 2008.

[9] H. R. Pant, D. R. Pandeya, K. T. Nam, W.-I. Baek, S. T. Hong, and H. Y. Kim, "Photocatalytic and antibacterial properties of a TiO_2/nylon-6 electrospun nanocomposite mat containing silver nanoparticles," *Journal of Hazardous Materials*, vol. 189, no. 1-2, pp. 465–471, 2011.

[10] G. M. Kuzmicheva, E. V. Savinkina, L. I. Belogorokhova, B. N. Mavrin, V. R. Flid, and A. G, "Yakovenko y A. I. Belogorokhov," *PHYSICAL CHEMISTRY OF NANOCLUSTERS AND NANOMATERIALS*, vol. 85, pp. 1138–1141, 2011.

[11] T. Gao, H. Fjeld, H. Fjellvag, T. Norby, and P. Norby, "In situstudies of structural stability and proton conductivity of titanate nanotubes," *Energy Environmental Science*, vol. 2, pp. 517–523, 2009.

[12] M. Qamar, C. R. Yoon, H. J. Oh et al., "Effect of post treatments on the structure and thermal stability of titanate nanotubes," *Nanotechnology*, vol. 17, no. 24, pp. 5922–5929, 2006.

[13] K. Matsubara and T. Tatsuma, "Morphological changes and multicolor photochromism of Ag nanoparticles deposited on single-crystalline TiO_2 surfaces," *Advanced Materials*, vol. 19, no. 19, pp. 2802–2806, 2007.

[14] S. L. Smitha, K. M. Nissamudeen, D. Philip, and K. G. Gopchandran, "Studies on surface plasmon resonance and photoluminescence of silver nanoparticles," *Spectrochimica Acta Part A: Molecular and Biomolecular Spectroscopy*, vol. 71, no. 1, pp. 186–190, 2008.

[15] D. C. Hurum, A. G. Agrios, K. A. Gray, T. Rajh, and M. C. Thurnauer, "Explaining the enhanced photocatalytic activity of Degussa P25 mixed-phase TiO_2 using EPR," *Journal of Physical Chemistry B*, vol. 107, no. 19, pp. 4545–4549, 2003.

[16] J. Yu and B. Wang, "Effect of calcination temperature on morphology and photoelectrochemical properties of anodized titanium dioxide nanotube arrays," *Applied Catalysis B: Environmental*, vol. 94, no. 3-4, pp. 295–302, 2010.

[17] K. S. W. Sing, "Reporting physisorption data for gas/solid systems with special reference to the determination of surface area and porosity (Recommendations 1984)," *Pure and Applied Chemistry*, vol. 57, no. 4, pp. 603–619, 1985.

[18] S. Bakardjieva, J. Šubrt, V. Štengl, M. J. Dianez, and M. J. Sayagues, "Photoactivity of anatase-rutile TiO_2 nanocrystalline mixtures obtained by heat treatment of homogeneously precipitated anatase," *Applied Catalysis B: Environmental*, vol. 58, no. 3-4, pp. 193–202, 2005.

[19] M. Hinojosa-Reyes, V. Rodríguez-González, and R. Zanella, "Gold nanoparticles supported on TiO_2-Ni as catalysts for hydrogen purification via water-gas shift reaction," *RSC Advances*, vol. 4, no. 9, pp. 4308–4316, 2014.

[20] M. Hinojosa-Reyes, A. Hernández-Gordillo, R. Zanella, and V. Rodríguez-González, "Renewable hydrogen harvest process by hydrazine as scavenging electron donor using gold TiO2 photocatalysts," *Catalysis Today*, vol. 266, pp. 2–8, 2016.

[21] V. Rodríguez-González, S. Obregón-Alfaro, L. M. Lozano-Sánchez, and S.-W. Lee, "Rapid microwave-assisted synthesis of one-dimensional silver-$H_2Ti_3O_7$ nanotubes," *Journal of Molecular Catalysis A: Chemical*, vol. 353-354, pp. 163–170, 2012.

[22] G. Guo, B. Yu, P. Yu, and X. Chen, "Synthesis and photocatalytic applications of Ag/TiO_2-nanotubes," *Talanta*, vol. 79, no. 3, pp. 570–575, 2009.

[23] H. Lin, X. Li, X. He, and J. Zhao, "Application of a novel 3D nano-network structure for Ag-modified TiO_2 film electrode with enhanced electrochemical performance," *Electrochimica Acta*, vol. 173, pp. 242–251, 2015.

[24] R. Camposeco, S. Castillo, J. Navarrete, and R. Gomez, "Synthesis, characterization and photocatalytic activity of TiO2 nanostructures: Nanotubes, nanofibers, nanowires and nanoparticles," *Catalysis Today*, vol. 266, pp. 90–101, 2016.

[25] R. Camposeco, S. Castillo, I. Mejia-Centeno, J. Navarrete, and R. Gómez, "Effect of the Ti/Na molar ratio on the acidity and the structure of TiO2 nanostructures: Nanotubes, nanofibers and nanowires," *Materials Characterization*, vol. 90, pp. 113–120, 2014.

[26] H. Yang, T. An, G. Li et al., "Photocatalytic degradation kinetics and mechanism of environmental pharmaceuticals in aqueous suspension of TiO2: A case of β-blockers," *Journal of Hazardous Materials*, vol. 179, no. 1-3, pp. 834–839, 2010.

[27] R. Amadelli, L. Samiolo, A. Maldotti, A. Molinari, and D. Gazzoli, "Selective photooxidation and photoreduction processes at Tio_2 surface-modified by grafted vanadyl," *International Journal of Photoenergy*, vol. 2011, Article ID 259453, 10 pages, 2011.